sustainability

MDPI

Article

Assessment of a Concealed Karst Cave's Influence on Karst Tunnel Stability: A Case Study of the Huaguoshan Tunnel, China

Xin Huang [1], Shucai Li [1], Zhenhao Xu [1,*], Ming Guo [2] and Yucheng Chen [3]

[1] Geotechnical and Structural Engineering Research Center, Shandong University, Jinan 250061, China; hx19891018@yeah.net (X.H); lishucai@sdu.edu.cn (S.L.)
[2] China Railway Engineering Consulting Group Co., Ltd., Zhengzhou 450001, China; goingmu@whu.edu.cn
[3] E-Xi Expressway Construction Headquarters of Hubei Province, Enshi 445000, China; yucheng_chen2018@163.com
* Correspondence: zhenhao_xu@sdu.edu.cn

Received: 23 May 2018; Accepted: 19 June 2018; Published: 22 June 2018

Abstract: In order to assess a concealed karst cave's influence on karst tunnel stability, an assessment model is proposed based on the analytic hierarchy process and a statistical analysis of relevant engineering projects. Major factors are studied and selected as impact factors of the assessment model based on a statistical analysis on a karst cave' s development conditions (karst hydrogeological and engineering geological conditions), construction conditions, and controlling measures. A weight analysis of factors shows that the surrounding rock grade, supporting measurement, formation lithology, unfavorable geology, construction methods, blasting techniques, advanced geological forecast, and groundwater level are the main controlling factors of the tunnel stability when there is a concealed karst cave in the tunnel. Topography and geomorphology, attitude of rocks, monitoring measurement, strata combination, and interlayer fissures are the minor influence factors. Tunnel section shapes, in situ stress, and geological logging are the least important factors. The proposed method is successfully applied to the assessment of a concealed karst cave's influence on the stability of the Huaguoshan Tunnel on the Enshi-Laifeng and Enshi-Qianjiang Expressways. The evaluation result agrees well with the construction site situation. In addition, the result provides good guidance with respect to the implementation of the treatment scheme and effectively avoids accidents in real-time.

Keywords: tunnel engineering; concealed karst cave; analytic hierarchy process method; factors' weight; stability assessment

1. Introduction

With the progressive implementation of the Western Development strategy in China, the construction of expressways, railways, and many other projects have entered a new period of development. Tens of thousands of kilometers of tunnels are, or will soon be, built in mountain areas of Western China [1]. The expressway project group of Western Hubei Province is located in Enshi Tujia and Miao Autonomous Prefecture and surrounding areas, which is one of the three major karst development areas in China. Karst develops in this region and the geological condition is complex, resulting in the difficulty of tunnel construction [2–5]. The construction risk is very high in karst areas [6–9]. In addition to the similar disasters happening in non-karst areas, there are always exit water and mud inrush, collapse, and other disasters in karst areas [10–13]. The disasters can cause significant casualties and economic losses [14–16]. The occurrence of these disasters is closely related to the development degree and the space form of the karst cave, as well as the karst water. The influences

of karst on tunnels are mainly the harm of karst water, karst caves, and the filling medium in the karst caves.

On one hand, karst water within the scope of the rock surrounding the tunnel can change the engineering geological and hydrogeological conditions in tunnels. It can cause a reduction in strength of the surrounding rock, a structural plane softening of the rock mass, an increase of the pore water pressure, and tunnel disasters, e.g., water and mud inrush [17–19]. Many scholars have performed a great deal of research on risk evaluation of water and mud inrush in karst tunnels [20–22]. Zhou et al. [23] established an optimal classification method based on grey system theory (GST) to evaluate the risk of water inrush and predict the occurrence probability in karst tunnels. Li et al. [24] put forward a method to evaluate the risk of water inrush in karst tunnels based on a synthetic attribute evaluation system.

On the other hand, because of the karst cave and the filling medium in it, an unloading effect of the surrounding rock occurred in the formation of karst caves. It changed the physical and mechanical properties of the surrounding rock and resulted in the change of the stress field and the displacement field [25–31]. A karst cave and the filling medium will make the construction mechanics more complex and easily cause excessive stress concentration in the surrounding rock, which results in an increase of deformation of the tunnel's surrounding rock [32,33]. The karst cave and the filling medium may cause the local surrounding rock to collapse and drop stones, which can endanger the safety of the construction staff and mechanical equipment, and even cause disasters, such as the tunnel roof collapse and blocking accidents [34,35]. A large number of studies on the influence of the karst cave on tunnel stability have been carried out. Taking a karst tunnel as an example, Wang and Sun [36] established a forecast model of the safe thickness of the karst cave floor. The model comprehensively reflected all the influence factors by using multiple regression and the support vector machine (SVM) method. Bian et al. [37] established a theoretical model for analyzing the mechanical characteristics of the surrounding rock in the karst-tunnel system. By using Schwarz's alternative method, the analysis solutions to the stress and deformation of the surrounding rock during excavating deep-buried tunnels under the existing karst cave conditions were derived. However, the former researchers merely studied the influence of the karst cave on the rock stability surrounding the tunnel from a single aspect and did not combine other factors, such as the reason for the development of the karst cave and the disturbance of the construction.

Based on the statistical analysis of 207 concealed karst caves in 21 tunnels of Enshi-Laifeng and Enshi-Qianjiang Expressways in Western Hubei Province, the influence factors of a karst cave on the tunnel stability are screened out by comprehensively considering the karst cave development conditions (karst engineering geological and hydrogeological conditions), the construction factors, and the early warning measurement. The assessment model for the stability of the rock surrounding the tunnel with a concealed karst cave is established by using the analytic hierarchy process. The corresponding early warning and control measures are taken against the risk to tunnel stability, which is caused by the karst cave. The study not only has an important technical value and economic significance to the tunnel construction in Western Hubei Province, but also has practical significance for survey, design, and construction of long tunnels under construction and to be built in karst areas.

2. Principle of Factors' Weight Analysis

The analytic hierarchy process (AHP) was developed by Saaty [38,39]. The AHP can make complex problems organized by dividing various factors into an associated order and hierarchy. According to some objective evaluation criterion, the relative importance of every two factors in each hierarchy is quantified, and the weights of all factors are determined [40].

The hierarchical analysis principle is based on a 1–9 scale method, as shown in Table 1. By comparing the relative importance between every two factors, a judgment matrix is established. By solving the characteristic roots of the judgment matrix, the largest characteristic root and the corresponding eigenvector can be obtained. The eigenvector is the ranking weight of the relative

importance of all factors in the same layer related to a certain factor in the upper layer. Finally, the consistency check is carried out. Equations (1)–(4) can be used in this process:

$$\overline{W_i} = (\prod_{j=1}^{n} A_{ij})^{1/n} (i = 1, 2, \cdots, n) \quad (1)$$

$$W_i = \overline{W}_i / \sum_{j=1}^{n} \overline{W_j} (i = 1, 2, \cdots, n) \quad (2)$$

$$\lambda_{\max} = (\sum_{i=1}^{n} ((AW)_i / W_i)/n \quad (3)$$

$$CI = (\lambda_{\max} - n)/(n-1) \quad (4)$$

$$CR = CI/RI \quad (5)$$

where W_i is a weight vector of the factors; A_{ij} is the judgment matrix; $\lambda_{\max}$ is the largest characteristic root of the judgment matrix; CI is the consistency index; and CR is random consistency ratio.

In order to ensure the objectivity of the judgment matrix, this paper studies the related engineering examples through the method of combining statistics and theoretical analyses. The hierarchical structure model is established, as shown in Figure 1. Through factor weight analysis, the relationship of different factors is studied, i.e., the influence degree of different factors on the safety thickness of a concealed cave in karst tunnels.

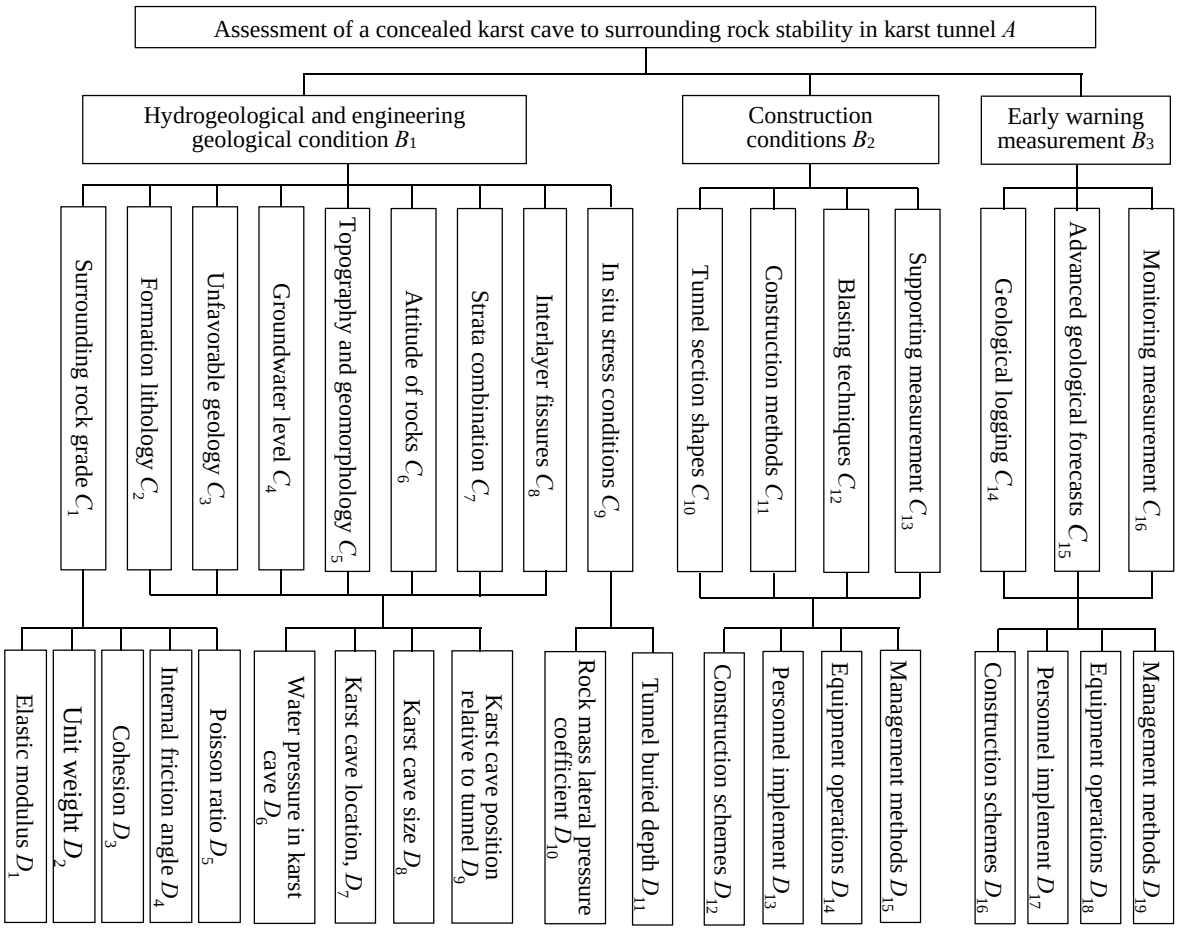

Figure 1. Hierarchical structure diagrams of assessment of a concealed karst cave to the rock surrounding the tunnel stability.

Table 1. Mean random consistency index (RI).

n	**1**	**2**	**3**	**4**	**5**	**6**	**7**	**8**	**9**
RI	0	0	0.52	0.89	1.12	1.26	1.36	1.41	1.46

3. Influence Factors and Weight Analysis

The stability analysis of a karst cave must consider the following two factors: The internal factors, including the burial depth, span, morphology, the position of the karst cave, water pressure in the karst cave, the attitude of rocks, the condition of joints and fissures, the physical and mechanical indices of the surrounding rock, and so on. The other are the external factors, including different kinds of construction disturbance, such as the duration of the disturbance, the load value, the dynamic load or static load, and so on. At the same time, the hydrogeological and engineering geological conditions in tunnel sites which influence the development process of karst caves should also be taken into consideration. Therefore, 207 karst caves' data of 21 tunnels of Enshi-Laifeng and Enshi-Qianjiang Expressways in Western Hubei Province are collected and organized systematically. The hydrogeological and engineering geological conditions of the tunnel sites, the construction conditions, and the appropriate warning measures are analyzed. The influence factors of the karst cave on tunnel stability are selected out, and their weights are analyzed, respectively. Finally, a complete evaluation system of the influence of a karst cave on the stability of the rock surrounding the tunnel under construction is established.

Among them, the judgment matrix of layer A to the factor of layer B is shown in Equation (6):

$$A_{A-B} = \begin{bmatrix} 1 & 2 & 5 \\ ½ & 1 & 3 \\ ⅕ & ⅓ & 1 \end{bmatrix} \quad (6)$$

The weight vector ($W_{A\text{-}B}$) is $[0.582, 0.309, 0.109]^{\mathrm{T}}$. The largest characteristic root ($\lambda_{\max}$) is 3.004. The consistency index (CI) is 0.002. The random consistency ratio meets the consistency requirements, i.e., $CR = 0.004 < 0.1$.

Karst hydrogeology and engineering geology are the material foundation and development environment of karst cave formation. The following influence factors are the important factors in the karst cave development and formation, including formation lithology, unfavorable geology, underground water, topography and geomorphology, attitude of rocks, strata combination, and interlayer fissures. These factors directly affect the location, shape, size, and the filling condition of a karst cave. They are the key influence factors to the stability of the rock surrounding the tunnel. Additionally, the surrounding rock grade and in situ stress condition are also important influence factors in this regard.

Different construction conditions will result in variations of physical and mechanical characteristics of the surrounding rock during the tunnel excavation process, which has an important influence on the surrounding rock stability. The construction conditions include different section shapes of a tunnel, different construction methods, different blasting techniques, and different corresponding supporting measurements.

Adopting reasonable early warning measurements can reduce the influence of the karst cave on the surrounding rock stability in the construction process. The early warning measures include geological logging, advanced geological forecasts, and monitoring measurement. Different construction schemes, workers, equipment, and management methods can cause different impacts on disaster early warnings. Therefore, construction schemes, personnel implementation, equipment operations, and management methods are selected in this paper to evaluate their influences in detail.

3.1. Hydrogeological and Engineering Geological Condition B_1

3.1.1. Surrounding Rock Grade C_1

There are many factors influencing the stability of the surrounding rock. Among which, the physical and mechanical properties of the surrounding rock are important factors for they can reflect the basic characteristics of the rock mass. If the surrounding rock is hard with good integrity, high strength, and highly resistant to deformation, it will show good stability during the tunnel construction and not easily break and deform. On the contrary, if the surrounding rock is weak and broken with low strength and weakly resistant to deformation, it is easy to break and deform acutely under the disturbance of construction. The physical and mechanical properties of the surrounding rock include five main parameters, namely unit weight, elastic modulus, Poisson ratio, internal friction angle and cohesion. Those five factors are adopted to evaluate the surrounding rock grade and their importance to the stability is divided into four levels, as shown in Table 2.

Table 2. Grade division of the surrounding rock.

Surrounding Rock Grades	Elastic Modulus *E* (GPa)	Unit Weight γ (kN/m^3)	Cohesion *C* (MPa)	Internal Friction Angle ϕ (°)	Poisson Ratio *v*	Stability
I, II	>20	25–28	>1.5	>50	<0.25	Strong
III	6–20	23–25	0.7–1.5	39–50	0.25–0.3	Medium
IV	1.3–6	20–23	0.2–0.7	27–39	0.3–0.35	Weak
V	1–2	17–20	0.05–0.2	20–27	0.35–0.45	Low

The judgment matrix is shown in Equation (7):

$$A_{C1-D} = \begin{bmatrix} 1 & 2 & 4 & 5 & 7 \\ ½ & 1 & 2 & 3 & 4 \\ ¼ & ½ & 1 & 2 & 3 \\ ⅕ & ⅓ & ½ & 1 & 2 \\ ⅐ & ¼ & ⅓ & ½ & 1 \end{bmatrix} \quad (7)$$

The weight vector ($W_{C1\text{-}D}$) is [0.467, 0.248, 0.143, 0.088, 0.054]$^{\mathrm{T}}$. The largest characteristic root ($\lambda_{\max}$) is 5.048. The consistency index (*CI*) is 0.012. The random consistency ratio meets the consistency requirements, i.e., $CR = 0.011 < 0.1$.

The result shows that the elastic modulus has the greatest weight in the influencing factors of the surrounding rock grade with a percentage of 46.7%. The unit weight ranks second with a percentage of 24.8%. The higher the elastic modulus and the unit weight are, the greater the strength and better stability of the surrounding rock are during the tunnel construction process.

3.1.2. Formation Lithology C_2

The karst development intensity is not identical with the change of the rock chemical composition. The lithology is the material basis of karst development, as well as a main factor to control the development and formation of a karst cave. Different lithology can cause great differentiation in the karst development even in the same geological conditions. In addition, the development morphology of the karst cave is different in various types of soluble rock stratum. The formation lithology is divided into four levels based on the influence of the karst development on the stability of the surrounding rock, as shown in Table 3.

Water pressure in the karst cave, and the location, shape, and size of the karst cave are analyzed, respectively. The judgment matrix is shown in Equation (8):

$$A_{C2-D} = \begin{bmatrix} 1 & 3 & 3 & 7 \\ ⅓ & 1 & 1 & 3 \\ ⅓ & 1 & 1 & 3 \\ ⅐ & ⅓ & ⅓ & 1 \end{bmatrix} \quad (8)$$

The weight vector ($W_{C2\text{-}D}$) is $[0.545, 0.193, 0.193, 0.069]^{\mathrm{T}}$. The largest characteristic root ($\lambda_{\max}$) is 4.008. The consistency index (CI) is 0.003. The random consistency ratio meets the consistency requirements, i.e., $CR = 0.003 < 0.1$.

Table 3. Grade division of formation lithology.

Grade Division	Lithology	Karst Development Degree	Stability
Non-soluble rock	Non-carbonate	Non-development	Strong
Weak soluble rock	Thin limestone, argillaceous limestone	Weak development	Medium
Medium soluble rock	Marble, dolomite	Medium development	Weak
Strong soluble rock	Thick-medium thick pure limestone, siliceous cementation dolomite, ampelitic limestone and limmer	Extremely development	Low

3.1.3. Unfavorable Geology C_3

A large number of joints and fissures develop in the surrounding rock of unfavorable geology. Furthermore, they will develop into water passages and hazard-causing structures under the effect of karst water. Unfavorable geology can also aggravate the karst development in karst areas, which has an important impact on the tunnel construction. Unfavorable geology is divided into four levels based on its potential for catastrophe with respect to the surrounding rock stability, i.e., strong potential, medium potential, weak potential, and non-potential for catastrophe.

Water pressure in the karst cave, and the location, shape, and size of the karst cave are analyzed respectively. The judgment matrix is shown in Equation (9):

$$A_{C3-D} = \begin{bmatrix} 1 & 2 & 3 & 7 \\ ½ & 1 & 1 & 3 \\ ⅓ & 1 & 1 & 3 \\ ⅐ & ⅓ & ⅓ & 1 \end{bmatrix} \quad (9)$$

The weight vector ($W_{C3\text{-}D}$) is $[0.508, 0.221, 0.200, 0.071]^{\mathrm{T}}$. The largest characteristic root ($\lambda_{\max}$) is 4.016. The consistency index (CI) is 0.005. The random consistency ratio meets the consistency requirements, i.e., $CR = 0.006 < 0.1$.

3.1.4. Groundwater Level C_4

The vertical hydrodynamic belt is an important factor to determine the distribution characteristics of the karst caves in karst areas. Down from the surface, four belts can be differentiated in the erosion karst in profile, namely the vertical vadose belt, seasonal variation belt, horizontal undercurrent belt, and deep slow flowing belt. The vertical vadose belt is above the water table, and the surface water is seepage vertically downward. Therefore, the karst phenomena, such as karst doline and sinkholes, always develop from the water table up to the surface. In the seasonal variation belt, groundwater is active and the karst process is strong. Therefore, the karst has stronger potential for catastrophe. The horizontal undercurrent belt is also called the shallow saturation belt, which is under the water table. There is perennial groundwater circulation and storage in this belt with high flow velocity and large flows. Groundwater has a strong corrosion capacity, so the horizontal undercurrent belt is the most favorable belt for karst development. The karst phenomena always appear along the groundwater flow direction, such as karst caves and dissolved fissures. The potential for catastrophe

is strong, too. The deep slow flowing belt is also called the deep saturation zone. The activity intensity of ground water lowers in this zone. The groundwater exists mainly in the form of pore water and fissure water. Due to the high groundwater level and water pressure in this zone, once the karst cave is revealed, water and mud inrush happens easily, which has a strong potential for catastrophe.

The karst water dynamic vertical belt is different with different elevations of the tunnel. Therefore, the groundwater is divided into four levels based on different height, i.e., h $\leq$ 10 m, 10 m < h $\leq$ 30 m, 30 m < h $\leq$ 60 m and h > 60 m, as shown in Table 4.

Table 4. Grade division based on elevation difference.

Elevation Difference *h*/m	Description	Karst Development Degree	Stability
H $\leq$ 0	Karst cave not filled with water, little potential for catastrophe	Non-development	Strong
0 < h $\leq$ 30	Lower water flow, lower water pressure, weak potential for catastrophe	Weak development	Medium
30 < h $\leq$ 60	Filled with water for a long time. Large water flow, high water flow velocity, high potential for catastrophe	Medium development	Weak
H > 60	High water pressure in karst cave, water and mud inrush happened once the karst revealed, extremely high potential for catastrophe	Extremely development	Low

Ditto, water pressure in the karst cave, the location, shape, and size of the karst cave are analyzed, respectively. The judgment matrix is shown in Equation (10):

$$A_{C4-D} = \begin{bmatrix} 1 & 3 & 5 & 7 \\ ⅓ & 1 & 1 & 3 \\ ⅕ & 1 & 1 & 3 \\ ⅐ & ⅓ & ⅓ & 1 \end{bmatrix} \quad (10)$$

The weight vector ($W_{C4\text{-}D}$) is $[0.589, 0.184, 0.162, 0.065]^{\mathrm{T}}$. The largest characteristic root ($\lambda_{\max}$) is 4.057. The consistency index (CI) is 0.019. The random consistency ratio meets the consistency requirements, i.e., CR = 0.021 < 0.1.

3.1.5. Topography and Geomorphology C_5

The lower the terrain is and the larger the catchment area is, the greater the benefit to the karst cave development. The surface water goes underground. The karst deep underground develops in the form of karst shafts, karst dolines, sinkholes, depressions, karst collapses, karst caves, trough valleys, and so on. The steeper the terrain is, the faster the surface water runoff. Therefore, water has difficulty entering the deep part. The karst develops mainly at the Earth's surface with a basic formation of surface erosion. The topography appears as clints, karrens, karst valleys, and so on. According to the catchment ability of the terrain and the karst development degree, topography and geomorphology can be divided into four levels: positive topography, small negative topography, medium negative topography, and large negative topography.

Ditto, water pressure in the karst cave, the location, shape, and size of the karst cave are analyzed, respectively. The judgment matrix is shown in Equation (11):

$$A_{C5-D} = \begin{bmatrix} 1 & 2 & 3 & 7 \\ ½ & 1 & 1 & 3 \\ ⅓ & 1 & 1 & 3 \\ ⅐ & ⅓ & ⅓ & 1 \end{bmatrix} \quad (11)$$

The weight vector ($W_{C5\text{-}D}$) is $[0.508, 0.221, 0.200, 0.071]^T$. The largest characteristic root (λ_{max}) is 4.016. The consistency index (CI) is 0.005. The random consistency ratio meets the consistency requirements, i.e., $CR = 0.006 < 0.1$.

3.1.6. Attitude of Rocks C_6

The development degree and extension direction of the corrosion fissure control the development degree, the direction, and size of a karst cave. Different dip angles of rock stratum can lead to different conditions of groundwater supply, runoff, discharge, and infiltration, as well as the karst development degree. Groundwater has a poor ability of infiltration in horizontal attitude rocks. The karst development is inhibited in this circumstance. The catchment area of vertical attitude rock strata is small. The water recycle is weak and the karst develops poorly in this circumstance. The dip angle of the rock stratum, which is most in favor of karst development, is 25°–65° of one wing of the syncline or the anticline [40]. According to different dip angles of the rock stratum and the karst development degree, the attitude of rocks is divided into four levels, as shown in Table 5.

Table 5. Grade division of attitude of rocks.

Dip Angle of Rock Stratum	Karst Development Degree	Stability
$0° \leq \phi < 10°$	Non-development	Strong
$80° \leq \phi \leq 90°$	Weak development	Medium
$10° \leq \phi < 25°$, $65° \leq \phi < 80°$	Medium development	Weak
$25° \leq \phi < 65°$	Extremely development	Low

Ditto, water pressure in the karst cave, the location, shape, and size of the karst cave are analyzed, respectively. The judgment matrix is shown in Equation (12):

$$A_{C6-D} = \begin{bmatrix} 1 & 3 & 3 & 7 \\ ⅓ & 1 & 1 & 3 \\ ⅓ & 1 & 1 & 3 \\ ⅐ & ⅓ & ⅓ & 1 \end{bmatrix} \quad (12)$$

The weight vector ($W_{C6\text{-}D}$) is $[0.545, 0.193, 0.193, 0.069]^T$. The largest characteristic root (λ_{max}) is 4.008. The consistency index (CI) is 0.003. The random consistency ratio meets the consistency requirements, i.e., $CR = 0.003 < 0.1$.

3.1.7. Strata Combination C_7

The development of the karst and its degree are closely related to the rock strata combination types. The soluble rock has a strong water permeability, while the non-soluble rock has a weak water permeability. When the former two rocks have different arrangements in the spatial position, the condition of groundwater runoff will change with it. Therefore, the karst development characteristics are also different. Soluble rock and non-soluble rock have three kinds of spatial position relationships, i.e., the soluble rock above the non-soluble rock, the soluble rock below the non-soluble rock, and the two rock strata interbedded with each other. The strata combination is divided into four levels, as shown in Table 6.

The contact zones of the soluble rock and the non-soluble rock are the places where the karst easily develops. Ditto, water pressure in the karst cave, the location, shape, and size of the karst cave are analyzed, respectively. The judgment matrix is shown in Equation (13):

$$A_{C7-D} = \begin{bmatrix} 1 & 3 & 3 & 5 \\ ⅓ & 1 & 1 & 3 \\ ⅓ & 1 & 1 & 3 \\ ⅕ & ⅓ & ⅓ & 1 \end{bmatrix} \quad (13)$$

The weight vector ($W_{C7\text{-}D}$) is [0.520, 0.201, 0.201, 0.078]^{T}. The largest characteristic root (λ_{max}) is 4.043. The consistency index (CI) is 0.014. The random consistency ratio meets the consistency requirements, i.e., CR = 0.016 < 0.1.

Table 6. Grade division of strata combination.

Grade Division	Description	Stability
Little favorable to karst development	Soluble rock with gentle attitude of rocks, below the non-soluble rock	Strong
Weak favorable to karst development	Soluble rock with gentle attitude of rocks, above the non-soluble rock, and the interface above the water table	Medium
Medium favorable to karst development	Soluble rock with gentle occurrence above the non-soluble rock, and the interface below the water table	Weak
Strong favorable to karst development	Steeply inclined or upright soluble rock interbedded with non-soluble rock	Low

3.1.8. Interlayer Fissures C_8

The karst effect is strong at the junction of structure joints and interlayer fissures. The development degree and extension directions of the fissures directly affect the activity and runoff conditions of the groundwater. Consequently, it can produce different influences on the development degree and the form of a karst cave. In general, karst most easily develops in the intersections or dense development regions of cracks. The interlayer fissures are divided into four levels, as shown in Table 7.

Table 7. Grade division of interlayer fissures.

Grade Division	Description	Stability
Little favorable to karst development	Weak-developed or non-developed at interlayer or interface	Strong
Weak favorable to karst development	Groundwater active in interlayer fissure well-developed position, karst well–developed	Medium
Medium favorable to karst development	Fissures developed in the middle-thick, thick, extra-thick limestone, different size karst caves well-developed	Weak
Strong favorable to karst development	Fissures developed in thin limestone, rock mass with lower load-bearing capacity, filled karst cave develop scatter sporadically, big karst cave system always developed on both sides	Low

Ditto, water pressure in the karst cave, the location, shape, and size of the karst cave are analyzed, respectively. The judgment matrix is shown in Equation (14):

$$A_{C8-D} = \begin{bmatrix} 1 & 3 & 3 & 7 \\ ⅓ & 1 & 1 & 3 \\ ⅓ & 1 & 1 & 3 \\ ⅐ & ⅓ & ⅓ & 1 \end{bmatrix} \quad (14)$$

The weight vector ($W_{C8\text{-}D}$) is [0.545, 0.193, 0.193, 0.069]^{T}. The largest characteristic root (λ_{max}) is 4.008. The consistency index (CI) is 0.003. The random consistency ratio meets the consistency requirements, i.e., CR = 0.003 < 0.1.

3.1.9. In Situ Stress Conditions C_9

The in situ stress is different when the tunnel is in different geographical environment. The depth of the tunnel has a close relationship with the vertical in situ stress. In general, the greater the depth is, the greater the in situ stress is, and the more detrimental it is to the stability of the rock surrounding the tunnel. The lateral pressure coefficient is an important index to describe the magnitude of horizontal in situ stress. When the lateral pressure coefficient varies, the stability state of the rock surrounding the tunnel will be different, too. When the tunnel is in the same depth, the stability of the surrounding rock gets worse with the increase of the lateral pressure coefficient. According to the difference of tunnel depth, lateral pressure coefficient, and their influences on the stability of the surrounding rock, the in situ stress condition is divided into four levels, as shown in Table 8.

Table 8. Grade division of in-situ stress condition.

Grade Division	Buried Depth D (m)	Lateral Pressure Coefficient λ	Stability
Low	$0 \leq D < 100$	$0 \leq \lambda < 1$	Strong
Medium	$100 \leq D < 300$	$1 \leq \lambda < 1.25$	Medium
High	$300 \leq D < 500$	$1.25 \leq \lambda < 1.5$	Weak
Rather high	$D > 500$	$1.5 \leq \lambda < 2$	Low

The buried depth and lateral pressure coefficient are analyzed, respectively. The judgment matrix is shown in Equation (15):

$$A_{C9-D} = \begin{bmatrix} 1 & 2 \\ ½ & 1 \end{bmatrix} \tag{15}$$

The weight vector ($W_{C9\text{-}D}$) is $[0.667, 0.333]^{\mathrm{T}}$. The largest characteristic root ($\lambda_{\max}$) is 2. The consistency (CI) index is 0. The random consistency ratio meets the consistency requirements, i.e., $CR = 0 < 0.1$.

Above all, the judgment matrix of the influence of a concealed karst cave on the surrounding rock stability is established, which involves all factors of hydrogeological and engineering geological conditions, as shown in Equation (16):

$$A_{B1-C} = \begin{bmatrix} 1 & 2 & 2 & 3 & 5 & 5 & 6 & 6 & 7 \\ ½ & 1 & 1 & 2 & 3 & 3 & 4 & 4 & 5 \\ ½ & 1 & 1 & 2 & 3 & 3 & 3 & 3 & 4 \\ ⅓ & ½ & ½ & 1 & 2 & 2 & 2 & 2 & 3 \\ ⅕ & ⅓ & ⅓ & ½ & 1 & 1 & 2 & 2 & 2 \\ ⅕ & ⅓ & ⅓ & ½ & 1 & 1 & 2 & 2 & 2 \\ \frac{1}{6} & ¼ & ⅓ & ½ & ½ & ½ & 1 & 1 & 2 \\ ⅙ & ¼ & ¼ & ½ & ½ & ½ & 1 & 1 & 2 \\ ⅐ & ⅕ & ¼ & ⅓ & ½ & ½ & ½ & ½ & 1 \end{bmatrix} \tag{16}$$

The weight vector ($W_{B1\text{-}C}$) is $[0.300, 0.179, 0.163, 0.100, 0.066, 0.066, 0.046, 0.046, 0.035]^{\mathrm{T}}$. The largest characteristic root ($\lambda_{\max}$) is 9.244. The consistency index (CI) is 0.031. The random consistency ratio meets the consistency requirements, i.e., $CR = 0.021 < 0.1$.

It can be seen that, surrounding rock grade, formation lithology, unfavorable geology, and groundwater level have the maximum influence on the stability of the surrounding rock with a concealed karst cave. The total weight of them accounts for 74.2%. The following are topography and geomorphology, attitude of rocks, strata combination, and interlayer fissures. They account for 22.3%. Additionally, the in situ stress, which accounts for 3.5%, is also one of the important factors influencing the stability of the rock surrounding the tunnel.

3.2. Construction Conditions B_2

The stability of the rock surrounding the tunnel is not only influenced by the mechanical property of the structural plan and body, as well as their situated environments, but also influenced by many construction factors, for example, the section shapes of the tunnel, the construction methods, blasting techniques, and supporting measurement. The construction is limited by human subjective factors with great uncertainty in them. All the construction schemes, operating workers, equipment, and organization management can greatly affect the construction. The stability of the surrounding rock will be good with reasonable construction plans, skilled operators, advanced equipment, and effective management ideas. Thus, construction schemes, personnel implementation, equipment operations, and management methods are selected in this layer. Four levels are established and used to evaluate the stability of the rock surrounding the tunnel, i.e., reasonable, basically reasonable, unreasonable, and extremely unreasonable.

3.2.1. Tunnel Section Shapes C_{10}

According to different geological conditions and construction requirements during the construction, different section shapes are selected. The most common section shapes of tunnels are the ellipse curve section, three-center-circle composite curve section, and three-center-circle fitting section. Selecting different section shapes of the tunnel can have different effects on the stability of the surrounding rock. The judgment matrix is shown in Equation (17):

$$A_{C10-D} = \begin{bmatrix} 1 & 2 & 3 & 2 \\ ½ & 1 & 2 & 1 \\ ⅓ & ½ & 1 & ½ \\ ½ & 1 & 2 & 1 \end{bmatrix} \quad (17)$$

The weight vector ($W_{C10\text{-}D}$) is $[0.423, 0.227, 0.122, 0.227]^{\mathrm{T}}$. The largest characteristic root ($\lambda_{\max}$) is 4.010. The consistency index (CI) is 0.003. The random consistency ratio meets the consistency requirements, i.e., $CR = 0.003 < 0.1$.

3.2.2. Construction Method C_{11}

Both the stress distribution and peripheral displacements in the rock surrounding the tunnel change constantly as the excavation proceeds. Therefore, different construction methods and sequences can cause significant differences in the surrounding rock stability. The judgment matrix is shown in Equation (18):

$$A_{C11-D} = \begin{bmatrix} 1 & 3 & 5 & 3 \\ ⅓ & 1 & 2 & 1 \\ ⅕ & ½ & 1 & ½ \\ ⅓ & 1 & 2 & 1 \end{bmatrix} \quad (18)$$

The weight vector ($W_{C11\text{-}D}$) is $[0.532, 0.186, 0.097, 0.186]^{\mathrm{T}}$. The largest characteristic root ($\lambda_{\max}$) is 4.004. The consistency index (CI) is 0.001. The random consistency ratio meets the consistency requirements, i.e., $CR = 0.001 < 0.1$.

3.2.3. Blasting Techniques C_{12}

The tunnel rock mass with a concealed karst cave are subjected to strong weathering, resulting in fragmented rock stratum and well-developed joints and fissures. In general, the blast can cause the destruction of the surrounding rock, which is more serious than that of the tunnel in non-karst regions. Therefore, adopting reasonable blasting methods, proper blasting length, and blasting with good quality can effectively reduce the blasting vibration damage to the surrounding rock, and avoid

serious accidents and disasters in the tunnel caused by a karst cave. The judgment matrix is shown in Equation (19):

$$A_{C12-D} = \begin{bmatrix} 1 & 3 & 5 & 2 \\ ⅓ & 1 & 2 & 1 \\ ⅕ & ½ & 1 & ⅓ \\ ½ & 1 & 3 & 1 \end{bmatrix} \quad (19)$$

The weight vector ($W_{C12\text{-}D}$) is $[0.490, 0.189, 0.089, 0.232]^{\mathrm{T}}$. The largest characteristic root (λ_{max}) is 4.025. The consistency index (CI) is 0.008. The random consistency ratio meets the consistency requirements, i.e., $CR = 0.009 < 0.1$.

3.2.4. Supporting Measurement C_{13}

Reasonable and timely supporting measures cannot only improve the stability of the surrounding rock during the excavation process, but also enhances the tunnel long-term stability. The judgment matrix is shown in Equation (19):

$$A_{C13-D} = \begin{bmatrix} 1 & 3 & 5 & 3 \\ ⅓ & 1 & 2 & 1 \\ ⅕ & ½ & 1 & ½ \\ ⅓ & 1 & 2 & 1 \end{bmatrix} \quad (20)$$

The weight vector ($W_{C13\text{-}D}$) is $[0.532, 0.186, 0.097, 0.186]^{\mathrm{T}}$. The largest characteristic root (λ_{max}) is 4.004. The consistency index (CI) is 0.001. The random consistency ratio meets the consistency requirements, i.e., $CR = 0.001 < 0.1$.

Above all, based on the engineering experience and theoretical analyses, the judgment matrix of the influence of a concealed karst cave on the surrounding rock stability is established and involves all of the factors of the construction condition mentioned above, as shown in Equation (21):

$$A_{B2-C} = \begin{bmatrix} 1 & 3 & 3 & 5 \\ ⅓ & 1 & 1 & 3 \\ ⅓ & 1 & 1 & 3 \\ ⅕ & ⅓ & ⅓ & 1 \end{bmatrix} \quad (21)$$

The weight vector ($W_{B2\text{-}C}$) is $[0.082, 0.235, 0.235, 0.449]^{\mathrm{T}}$. The largest characteristic root (λ_{max}) is 4.004. The consistency index (CI) is 0.001. The random consistency ratio meets the consistency requirements, i.e., $CR = 0.001 < 0.1$.

It can be seen that supporting measurement has the greatest influence on surrounding rock stability. Its weight accounts for 44.9% of all factors. Construction methods and blasting techniques are secondary. Both of them account for 23.5%. Finally, the section shape accounts for 8.2%.

3.3. Early Warning Measurement B_3

Adopting reasonable construction control measures can reduce the destruction of the surrounding rock during the construction process. In the influence evaluation of a concealed karst cave on the stability of the rock surrounding the tunnel, geological logging, advanced geological forecasts, and monitoring measurements are taken as the main early warning measures. Thus, construction schemes, personnel implementation, equipment operations, and management methods are selected in this layer. Four levels are established and used to evaluate the stability of the rock surrounding the tunnel, i.e., reasonable, basically reasonable, unreasonable, and extremely unreasonable.

3.3.1. Geological Logging C_{14}

The judgment matrix is shown in Equation (22):

$$A_{C14-D} = \begin{bmatrix} 1 & 2 & 5 & 2 \\ ½ & 1 & 2 & 1 \\ ⅕ & ½ & 1 & ½ \\ ½ & 1 & 2 & 1 \end{bmatrix} \quad (22)$$

The weight vector ($W_{C14\text{-}D}$) is $[0.461, 0.218, 0.103, 0.218]^T$. The largest characteristic root (λ_{max}) is 4.006. The consistency index (CI) is 0.002. The random consistency ratio meets the consistency requirements, i.e., $CR = 0.002 < 0.1$.

3.3.2. Advanced Geological Forecasts C_{15}

The judgment matrix is shown in Equation (23):

$$A_{C15-D} = \begin{bmatrix} 1 & 2 & 4 & 3 \\ ½ & 1 & 2 & 2 \\ ¼ & ½ & 1 & ½ \\ ⅓ & ½ & 2 & 1 \end{bmatrix} \quad (23)$$

The weight vector ($W_{C15\text{-}D}$) is $[0.475, 0.255, 0.107, 0.163]^T$. The largest characteristic root (λ_{max}) is 4.046. The consistency index (CI) is 0.015. The random consistency ratio meets the consistency requirements, i.e., $CR = 0.017 < 0.1$.

3.3.3. Monitoring Measurement C_{16}

The judgment matrix is shown in Equation (24):

$$A_{C16-D} = \begin{bmatrix} 1 & 3 & 5 & 3 \\ ⅓ & 1 & 2 & 1 \\ ⅕ & ½ & 1 & ½ \\ ⅓ & 1 & 2 & 1 \end{bmatrix} \quad (24)$$

The weight vector ($W_{C16\text{-}D}$) is $[0.532, 0.186, 0.097, 0.186]^T$. The largest characteristic root (λ_{max}) is 4.004. The consistency index (CI) is 0.001. The random consistency ratio meets the consistency requirements, i.e., $CR = 0.001 < 0.1$.

Above all, based on the engineering experience and theoretical analyses, the judgment matrix of the influence of a concealed karst cave on the stability of the surrounding rock is established and involves all factors of early warning measures, as shown in Equation (25):

$$A_{B3-C} = \begin{bmatrix} 1 & ⅕ & ⅓ \\ 5 & 1 & 2 \\ 3 & ½ & 1 \end{bmatrix} \quad (25)$$

The weight vector ($W_{B3\text{-}C}$) is $[0.109, 0.582, 0.309]^T$. The largest characteristic root (λ_{max}) is 3.004. The consistency index (CI) is 0.002. The random consistency ratio meets the consistency requirements, i.e., $CR = 0.004 < 0.1$.

The early warning measurements of the tunnels with a concealed karst cave are different from that of common mountain tunnels. Advanced geological forecasts are more important than other control measures, because the karst development forms and the filling conditions are unknown before it is revealed, which poses a great threat to the stability of the rock surrounding the tunnel. Therefore, the weight of the advanced geological forecasts accounts for 58.2% of all factors. The monitoring

measurement can provide feedback of the stability of the surrounding rock in real-time and give early warnings of the danger zones in a timely manner. The weight of the monitoring measurement accounts for 30.9%. The geological logging can record the revealed form of the tunnel face and provide feedback in real-time, as well, which also has an important influence on the stability of the rock surrounding the tunnel.

3.4. Evaluation Index and Classification Criterion

Based on the above analyses, the assessment indices and classification standards are confirmed, as shown in Table 9.

Table 9. Assessment indices and classification standard.

Factors	Stability Grade			
	I Stable	**II Basic Stable**	**III Unstable**	**IV Extremely Unstable**
Surrounding rock grade	I, II	III	IV	V
Formation lithology	Non-soluble rock	Weak soluble rock	Medium soluble rock	Strong soluble rock
Unfavorable geology	Non-potential for catastrophe	Weak potential for catastrophe	Medium potential for catastrophe	Strong potential for catastrophe
Ground water level	H < 0	0 < h ≤ 30	30 < h ≤ 60	H > 60
Topography and geomorphology	Positive topography	Small negative topography	Medium negative topography	Large negative topography
Attitude of rocks (dip angle ϕ)	0° ≤ ϕ < 10°	80° ≤ ϕ ≤ 90°	10° ≤ ϕ < 25° 65° ≤ ϕ < 80°	25° ≤ ϕ < 65°
Strata combination	Little favorable to karst development	Weak favorable to karst development	Medium favorable to karst development	Strong favorable to karst development
Interlayer fissures	Little favorable to karst development	Weak favorable to karst development	Medium favorable to karst development	Strong favorable to karst development
In-situ stress condition	Low	Medium	High	Rather high
Tunnel section shapes	Reasonable	Basically reasonable	Unreasonable	Extremely unreasonable
Construction methods	Reasonable	Basically reasonable	Unreasonable	Extremely unreasonable
Blasting techniques	Reasonable	Basically reasonable	Unreasonable	Extremely unreasonable
Supporting measurement	Reasonable	Basically reasonable	Unreasonable	Extremely unreasonable
Geological logging	Reasonable	Basically reasonable	Unreasonable	Extremely unreasonable
Advanced geological forecasts	Reasonable	Basically reasonable	Unreasonable	Extremely unreasonable
Monitoring measurement	Reasonable	Basically reasonable	Unreasonable	Extremely unreasonable

4. General Ranking of Influence Factors and Weight Analysis

4.1. General Ranking of Influence Factors

Supposing that the weights of the m factors in the $k-1$ layer relative to the general goal are worked out as $W^{(k-1)} = (W_1{}^{(k-1)}, W_2{}^{(k-1)}, \ldots, W_m{}^{(k-1)})^T$, let $P^{(k)} = \left(p_1{}^{(k)}, p_2{}^{(k)}, \ldots, p_n{}^{(k)}\right)$, which represents the ranking of the k layer to the $k-1$ layer [40]. Therefore, the general ranking of the factors in k layer relative to general goal can be obtained by Equation (26):

$$Wi^{(k)} = \sum_{j=1}^{m} pij^{(k)} Wj^{(k-1)} \ (i = 1, 2, \cdots, n) \tag{26}$$

The comprehensive check index of the k layer is obtained by Equations (27)–(29):

$$CI_j{}^{(k)} = (CI_1{}^{(k)}, CI_2{}^{(k)}, \ldots, \mathrm{CI}_m{}^{(k)}) W^{(k-1)} \tag{27}$$

$$RI_j^{(k)} = (RI_1^{(k)}, RI_2^{(k)}, \ldots, RI_m^{(k)})W^{(k-1)} \quad (28)$$

$$CR^{(k)} = CI^{(k)}/RI^{(k)} \quad (29)$$

When $CR^{(k)} < 0.1$, the global consistency of the judgment matrix is acceptable.

4.1.1. General Ranking of Influence Factors in Layer *C*

The factors in layer *C* are from C_1 to C_{16} and the general ranking is shown in Figure 2. The weight vector of general ranking ($\omega_{B\text{-}C}$) is [0.174, 0.104, 0.095, 0.058, 0.038, 0.038, 0.027, 0.027, 0.020, 0.025, 0.073, 0.073, 0.139, 0.012, 0.064, 0.034]^T, and CI = 0.018, RI = 1.181, CR = 0.015 < 0.1. It meets the consistency requirements.

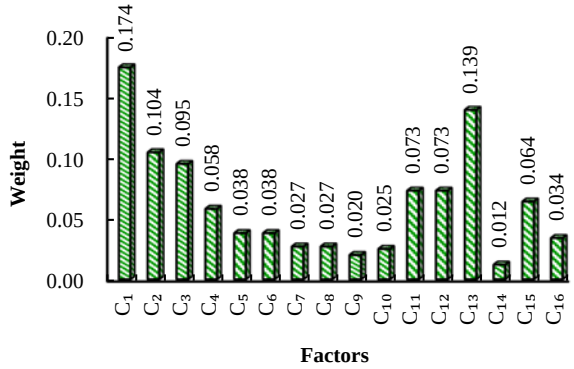

Figure 2. Factors' weight histogram of layer *C*.

4.1.2. General Ranking of Influence Factors in Layer *D*

The factors in layer *D* are from D_1 to D_{19} and the general ranking is shown in Figure 3. The weight vector of general ranking ($\omega_{C\text{-}D}$) is [0.081, 0.043, 0.025, 0.015, 0.009, 0.208, 0.078, 0.074, 0.027, 0.014, 0.007, 0.159, 0.059, 0.030, 0.062, 0.054, 0.025, 0.011, 0.019]^T, and CI = 0.007, RI = 0.912, CR = 0.008 < 0.1. It meets the consistency requirements.

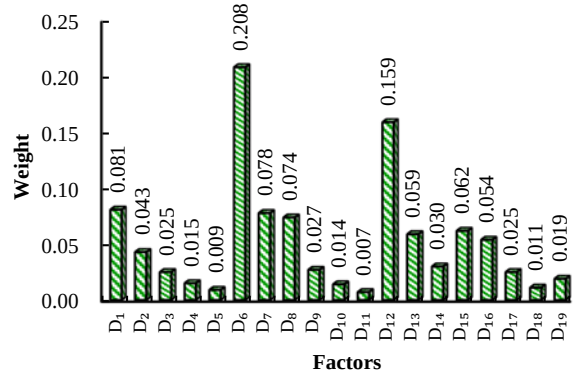

Figure 3. Factors' weight histogram of layer *D*.

4.2. Weight Analysis

The weight of the factors in layer C from large to small in turn is $\omega_{C1} > \omega_{C13} > \omega_{C2} > \omega_{C3} > \omega_{C11} = \omega_{C12} > \omega_{C15} > \omega_{C4} > \omega_{C5} = \omega_{C6} > \omega_{C16} > \omega_{C7} = \omega_{C8} > \omega_{C10} > \omega_{C9} > \omega_{C14}$. Surrounding rock grades, formation lithology, supporting measurement, formation lithology, unfavorable geology, construction methods, blasting techniques, advanced geological forecasts, and ground water levels have the most impact on the stability of the tunnel with a concealed karst cave, and the sum of these factors' weights account for 77.9%. The secondary influence factors are topography and geomorphology, attitude of

rocks, monitoring measurement, strata combination, and interlayer fissures with a total percentage of 16.3%. Finally, other influence factors, such as geo-stress conditions, section shapes, and geological logging, have a relatively small impact on the stability of the tunnel with a concealed karst cave, and the sum of these factors' weights account for 5.8%.

The weights of the factors in layer *D* from large to small, in turn, are $\omega_{D6} > \omega_{D12} > \omega_{D1} > \omega_{D7} > \omega_{D8} > \omega_{D15} > \omega_{D13} > \omega_{D16} > \omega_{D2} > \omega_{D14} > \omega_{D9} > \omega_{D3} = \omega_{D17} > \omega_{D19} > \omega_{D4} > \omega_{D10} > \omega_{D18} > \omega_{D5} > \omega_{D11}$. The water pressure in the karst cave, construction schemes, elastic modulus, karst cave shapes, karst cave sizes, construction organization and management, construction personnel implementation, and early-warning schemes have the most impact on the stability of the tunnel with a concealed karst cave. The sum of these factors' weights account for 77.5%. The secondary influence factors are the unit weight of the rock mass, construction equipment, the karst cave location relative to tunnels, cohesion, and early warning personnel implementation with a total percentage of 15%. Finally, other influence factors, such as the early warning organization and management, internal friction angles, lateral pressure coefficient, early warning equipment, Poisson ratio, and tunnel depth have a relatively small impact on the stability of the tunnel with a concealed karst cave and the sum of these factors' weights account for 7.6%.

4.3. Stability Assessment

The stability classification of a concealed karst cave's influence on the rock surrounding the tunnel can be obtained from Equations (30)–(32), which is the sum of every factor's expert grade multiplied by the corresponding weight, respectively [40]:

$$A = [a_1 a_2 \cdots a_i \cdots a_n] \tag{30}$$

$$W = [\omega_1 \omega_2 \cdots \omega_i \cdots \omega_n]^T \tag{31}$$

$$S = A \cdot W \tag{32}$$

where A refers to the expert grade vector; W is the weight vector of the factors; and S is the grading value of the stability.

The value of expert grade vector can be obtained according to the grade division of the influence factors, as shown in Table 10.

Table 10. Grade division of the influence factors.

Grade	I	II	III	IV
Values	$75 \leq S \leq 100$	$50 \leq S < 75$	$25 \leq S < 50$	$0 \leq S < 25$

The weight vector of the factors can be assessed and graded by weighting the two kinds of factors in layer C and layer *D*.

The expert grade vector can be obtained by the confidence index method [40]. The confidence index ζ is a value between the interval [0, 10] acquired by the experts based on their research achievements and experience. It can reflect the probability information of the data reliability and objectivity. For example, when the expert's conclusion is grade III: $S = 49$, and the confidence index is 8.8. This indicates that the expert considers that the percentage of the tunnel stability in grade III is 88%. Finally, the stability grade and probability distribution can be obtained by comprehensive statistical analyses of the probability given by different experts in the expert database and overlaying the probability distribution.

5. Engineering Application

5.1. General Situation of the Project

Huaguoshan Tunnel is one of the main projects of the Enshi-Qianjiang Expressway, located in Xianfeng County, Enshi Tujia and Miao Autonomous Prefecture Hubei Province as a separated tunnel. The left tunnel is 3254 m long, starting from ZK94 + 362 to ZK97 + 616, and the right tunnel is 3221 m long, starting from YK94 + 365 to YK97 + 586. The maximum depth of the tunnel is 160 m. The axis azimuth of both the entrance and the exit is about 274°. The tunnel site is located in Jiamachi town, Xianfeng County, and belongs to the landform of a medium-low mountain area with structural corrosion and erosion. The tunnel passes through multiple adjacent mountains with a generally smooth terrain, which are residual hills after dissolution and denudation. Mountains are in a round shape and develop with many karst depressions. Part of the tunnel is covered with thick layers. The underlying bedrock are Lower Permian Qixia Formation limestone, Lower Permian Maokou Formation limestone, carbonaceous limestone, and limestone with intercalation of thin layer shale, which are soluble carbonate rock. The karst develops in the depth of the mountain, and there are many nearly perpendicular karst passages. Several of the karst passages are near the vault of the tunnel, and may communicate with the tunnel. The karst conduits collect and discharge surface water and are filled with breccia and cohesive soil carried by groundwater. The attitude of rocks in the area is stable. The groundwater is rich, and the karst is well-developed. The geological disasters easily break out during the construction, such as large water inrush, mud inrush, and landslides.

5.2. Influence Factors and Surrounding Rock Stability Classification

When the left tunnel was excavated at ZK96 + 794 on 2 January 2013, two karst caves were revealed at the left arch foot and the right arch haunch of the tunnel, as shown in Figures 4 and 5. The original design of the support is of the SF-II type. The surrounding rock are medium-thick layers slightly weathered limestone with intercalations of carbonaceous limestone. The surrounding rock is dominated by hard rock, and a few fractures of the rock mass develop here. The rock mass maintains its comparative integrity and presents as blocky structures. The arch is basically stable. The strata are gentle, and a small amount of rock blocks fall along the bedding plane. The groundwater is poor. The tunnel is generally dry, but there is dripping in the rainy season. The practically-revealed surrounding rock is moderately weathered limestone of medium-thick structure with intercalations of strongly weathered shale at the tunnel face. Part of the shale is strongly weathered and presents as a loosed soil structure. The dip angle of the strata is 10°–15°. The joints and fissures are well developed. The fissures are open and filled with silty clay. The surrounding rock is from comparatively broken to broken. The tunnel is about 160 m deep in this section and there are several buildings on the Earth's surface above the karst cave areas. The karst cave is located at a transverse traffic tube (ZK96 + 796), which is in front of the tunnel face and develops squinted down along the small mileage. The lowest of the karst cave and the tunnel floor are basically on the same level. A karst shaft develops at the ZK96 + 746 section and intersects the tunnel hole axis at an angle of about 43°. The longitudinal length of the shaft is 11.0 m at the tunnel axis and the shaft extends to the left of the tunnel face (the right tunnel direction). The shaft connects the karst cave at YK96 + 766 of the right hole through corrosion fissure. There is no special smell in the hole. The floor of the karst cave is so smooth and slippery that it is difficult to walk on it.

Based on above engineering data, and according to the assessment indices and classification standards in Table 9, the expert grading values of the influence factors from C1 to C16 can be obtained.

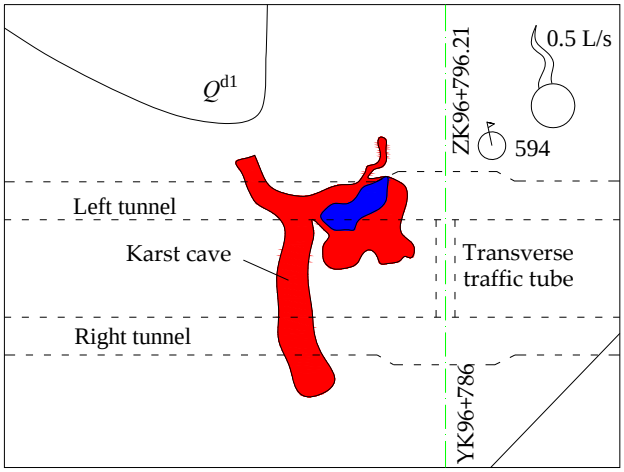

Figure 4. Plan sketch of the karst cave position.

Figure 5. Revealed karst cave on the tunnel face.

5.2.1. Surrounding Rock Grade C_1

The original design of the surrounding rock from ZK96 + 535 to ZK97 + 155 is level II. Actually, the revealed surrounding rock from ZK96 + 720 to ZK96 + 824 is level IV. In Table 9, when the surrounding rock grade is IV, the corresponding stability grade is III, i.e., unstable. Then, according to Table 10, the expert grading value of the surrounding rock grade (C_1) is obtained, i.e., a_1 = 26.

5.2.2. Formation Lithology C_2

The revealed surrounding rock is Qixia Formation moderately weathered limestone with intercalation of thin layer strongly-weathered shale at the tunnel face. Part of the shale is strongly weathered and presents as loosed soil structures with extremely low strength. The limestone is hard rock and belongs to soluble carbonatite. It belongs to strong development karst layer. In Table 9, the corresponding stability grade of the strong development karst layer is IV, i.e., extremely unstable. Then according to Table 10, the expert grading value of formation lithology (C_2) is obtained, i.e., a_2 = 9.

5.2.3. Unfavorable Geology C_3

There are many nearly-perpendicular karst passages. Several of the karst passages are near the vault of the tunnel and may communicate with the tunnel. The karst passages gather and discharge surface water and are filled with breccia and cohesive soil carried by groundwater. Water inflows, mud inrush, sand inflows, and other disasters are very likely to happen in the tunnel when it rains.

It has strong potential for catastrophe. In Table 9, the corresponding stability grade of unfavorable geology with strong potential for catastrophe is IV, i.e., extremely unstable. Then, according to Table 10, the expert grading value of unfavorable geology (C_3) is obtained, i.e., a_3 = 16.

5.2.4. Groundwater Level C_4

The designed water table is 70–80 m higher than the tunnel floor. According to Table 9, the corresponding stability grade of the groundwater level is IV, i.e., extremely unstable. Then, according to Table 10, the expert grading value of the groundwater level (C_4) is obtained, i.e., a_4 = 15.

5.2.5. Topography and Geomorphology C_5

There are multiple karst depressions, rough valleys, sinkholes, and karst funnels on the Earth's surface near ZK96 + 796. They are related to the Huaguoshan Tunnel karst water systems. The karst depressions present as a "scoop" shape, and the terrain is flat and filled with cohesive soil. There are two sinkholes developing in the karst depressions. The first place is the drainage passage of the surface water. It drains the water from the farmland during the rainy season and has no surface water in the dry season. The sinkhole is located at the contact region of the mountain and the edge of the intermountain depression. The hole appears as an oval and it is 5–6 m long, and 4–5 m wide. It tilts downward. The extending direction is 335°, and the angle of inclination is about 60°. The visible depth is about 9 m. The diameter at the bottom within the visible depth is 3.5 m. The rock mass around the hole is of medium-thick layer limestone, and the attitude of strata is 330°∠11°. The second sinkhole is about 1.5 m in diameter. It was buried by the cohesive soil when the steep hill collapsed in 2010. It is the drainage passage of the surface water in the karst depression during the rainy season and belongs to the large negative topography. In Table 9, the corresponding stability grade of the large negative topography is IV, i.e., extremely unstable. Then, according to Table 10, the expert grading value of the topography and geomorphology (C_5) is obtained, i.e., a_5 = 18.

5.2.6. Attitude of Rocks C_6

The dip angle of strata is 10°–15°. In Table 9, the corresponding stability grade is III, i.e., unstable. Then, according to Table 10, the expert grading value of attitude of rocks (C_6) is obtained, i.e., a_6 = 47.

5.2.7. Strata Combination C_7

The underlying bedrock are Lower Permian Qixia Formation limestone, thin layer shale, Lower Permian Maokou Formation limestone, and carbonaceous limestone. The fissures are filled with silty clay. The combination degree of the interlayer is poor. It belongs to the area that is strongly favorable to karst development. In Table 9, the corresponding stability grade is IV, i.e., extremely unstable. Then, according to Table 10, the expert grading value of the strata combination (C_7) is obtained, i.e., a_7 = 10.

5.2.8. Interlayer Fissures C_8

The surrounding rock is comparatively broken. The joints and fissures extremely develop. The fissures are filled with silty clay. The combination degree of the interlayer is poor. It belongs to the area that is strongly favorable to karst development. In Table 9, the corresponding stability grade is IV, i.e., extremely unstable. Then, according to Table 10, the expert grading value of Interlayer fissures (C_8) is obtained, i.e., a_8 = 21.

5.2.9. In Situ Stress Conditions C_9

The buried depth is about 160 m. The grade division is medium, according to Table 8. In Table 9, the corresponding stability grade is II, i.e., basically stable. Then, according to Table 10, the expert grading value of in situ stress conditions (C_9) is obtained, i.e., a_9 = 57.

5.2.10. Tunnel Section Shapes C_{10}

The single centered circular of which the radius is 5.5 m is chosen as the tunnel inside lining shape. The selected tunnel section shape is reasonable. In Table 9, the corresponding stability grade is I, i.e., stable. Then, according to Table 10, the expert grading value of tunnel section shapes (C_{10}) is obtained, i.e., a_{10} = 80.

5.2.11. Construction Methods C_{11}

In the original design, the tunnel construction is based on level II surrounding rock. However, the revealed surrounding rock does not meet the requirement, and the actual construction is based on level IV surrounding rock. Therefore, the initially-selected construction method is extremely unreasonable. In Table 9, the corresponding stability grade is IV, i.e., extremely unstable. Then, based on Table 10, the expert grading value of construction methods (C_{11}) is obtained, i.e., a_{11} = 23.

5.2.12. Blasting Techniques C_{12}

In the original design, the excavation method is smooth blasting, and the cyclical footage is 3 m. After revealing the karst cave, the surrounding rock grade adjusts to level IV. Thus, the method of short footage and weak blasting should be adopted during the tunnel excavation. Therefore, in Table 9, the initially-selected blasting method is unreasonable. The corresponding stability grade is III, i.e., unstable. Then, based on Table 10, the expert grading value of blasting techniques (C_{12}) is obtained, i.e., a_{12} = 37.

5.2.13. Supporting Measurement C_{13}

The original design is a SF-II type support. After revealing the karst cave, the support scheme changes to SF-IVc. The I beams change from no. 14 to no. 18. The longitudinal space of the I beams and system rock bolts adjust to 0.6 m. The excavation section is expanded accordingly. The thickness of the spray concrete is 24 cm. In addition, the advanced small pipe method is adopted as auxiliary construction. Other parameters are the same as the parameters of the SF-IVc type support. In Table 9, the original supporting measurement is extremely unreasonable and the corresponding stability grade is IV, i.e., extremely unstable. According to Table 10, the expert grading value of blasting techniques (C_{13}) is obtained, i.e., a_{13} = 14.

5.2.14. Geological Logging C_{14}

The previous geological investigation has proved that the karst conduits are filled with breccia and cohesive soil carried by groundwater. Water inflows, mud inrush, and sand inflows are very likely to happen in the tunnel when it rains. The geological logging should be reinforced during tunnel construction but, actually, correlative data are insufficient in this process. Therefore, it is extremely unreasonable and the corresponding stability grade is IV, i.e., extremely unstable. According to Table 10, the expert grading value of geological logging (C_{14}) is obtained, i.e., a_{14} = 15.

5.2.15. Advanced Geological Forecasts C_{15}

This segment is special and dangerous. Long distance detection (tunnel seismic forecast) and short distance detection (geological radar detection) should be combined, and more detection methods should be taken, such as the geological analysis, the electrical method, and the transient electromagnetic method. The original advanced geological forecasts is unreasonable, and the corresponding stability grade is III, i.e., unstable. Then according to Table 10, the expert grading value of advanced geological forecasts (C_{15}) is obtained, i.e., a_{15} = 37.

5.2.16. Monitoring Measurement C_{16}

The segment should be monitored frequently, and auxiliary monitoring measures should be taken as well. Therefore, the monitoring measurement is unreasonable. In Table 9, the corresponding stability

grade is III, i.e., unstable. Then according to Table 10, the expert grading value of the monitoring measurement (C_{16}) is obtained, i.e., a_{16} = 31.

To sum up, the expert grading vector is obtained as shown in Equation (33):

$$A = \{26\ 9\ 16\ 15\ 18\ 47\ 10\ 21\ 57\ 80\ 23\ 37\ 14\ 15\ 37\ 31\} \quad (33)$$

Finally, the grading value of the stability is obtained by substituting Equation (32) into Equation (24), i.e., S = 24.225. The surrounding rock is extremely unstable and the grade is IV. Collapse and other accidents are prone to happen in this area.

5.3. Revealed Condition of the Karst Cave

The fully-revealed karst cave at ZK96 + 746 of the Huaguoshan Tunnel at the Qianjiang segment is shown in Figure 6. The entry is a vertical shaft which is about 322 m deep, 23.3 m wide, and 11 m long. The entry is located at the left of the tunnel. The elevation of the tunnel floor is 807 m and the elevation of the shaft bottom is 485 m, as shown in Figure 6c. The investigation shows that a medium groundwater passage develops in the vertical shaft and passes through the left hole and right hole of the Huanguoshan Tunnel. The top of the underground river is 330 m from the bottom of the tunnel. The capacity of the shaft is 150,693 m^3. The surface area of the shaft is 630 m^2. A large area of collapse happened at the karst cave and the tunnel top along the large mileage direction after the karst cave was revealed. The internal cavity is in unstable condition with frequent dropping or falling stones. The surrounding rock at the top of the tunnel is moderately weathered limestone and presents thin and medium-thick layer structures. The attitude is gentle and close to horizontal. The interlayer bond strength is poor, and the top is extremely unstable. It brings about great hidden dangers to construction safety. The verification of excavating coincides with the calculation result, which proves that it is reasonable and feasible to use the analytic hierarchy process to evaluate the stability of the rock surrounding the tunnel.

(**a**) Collapse condition of the karst hall

(**b**) Collapse and dropping stones

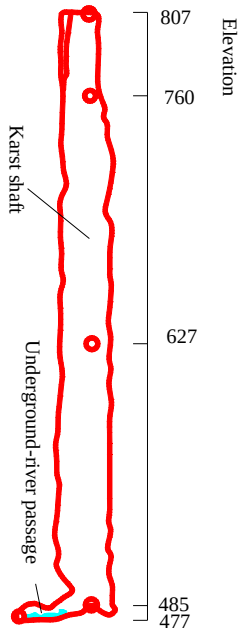

(**c**) Sketch map of the karst shaft

Figure 6. The completely revealed condition of the karst cave at ZK96 + 746.

5.4. Treatment Measure of the Karst Cave

Since the development scale of the karst cave is very large, and the construction risk is very high, the treatment should be divided into different stages, different positions with gradualness from easy ones to difficult ones. Therefore, the treatment process from ZK96 + 732 to ZK96 + 752 was divided into four stages: backfill of the karst cave shaft, protection arch construction, bridge crossing the shaft construction, and secondary lining construction. The schematic diagrams of the karst cave treatment are shown in Figures 7 and 8.

(1) Backfill of the Karst Cave Shaft

The total amount of the backfill was 156,130 m^3. Tunnel mucking with good water permeability was preferred to backfill the karst cave shaft, and the inadequate portion used the mucking from the abandoned mucking sites out of the tunnel.

(2) Protection Arch Construction

The arch construction mileage was 20 m long, which is from ZK96 + 732 to ZK96 + 752. The specific constructions are as follows:

In the premise of safety, the rock mass exceeding clearance limit at both ends of the karst cave were excavated to the profile outline outside of the protection arch. The breaking hammer was used in the process because blasting would cause a serious disturbance to the karst cave.

A shotcrete-rock bolt-mesh support technique was taken to support the inner wall of the karst cave from the arch foot to the place 4 m above the tunnel vault. The ϕ22 grouted rock bolts were 4.5 m long and were arranged at the spacing of 1.0 m × 1.0 m and presented as a plum blossom mold layout. The ϕ8 steel mesh was at the spacing of 25 cm × 25 cm. The thickness of C20 shotcrete was 10 cm. The inner wall above the 4 m tunnel vault was only supported by using C20 shotcrete 10 cm in thickness.

Then excavation of the bridge abutment with the breaking hammer was performed and the construction of bridge abutment cap, cushion block and so on, were finished.

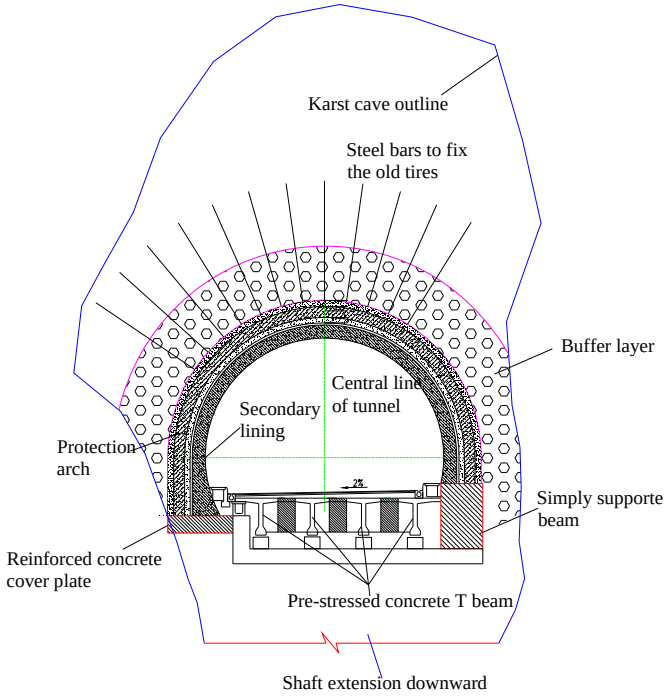

Figure 7. Schematic diagram of the karst cave treatment.

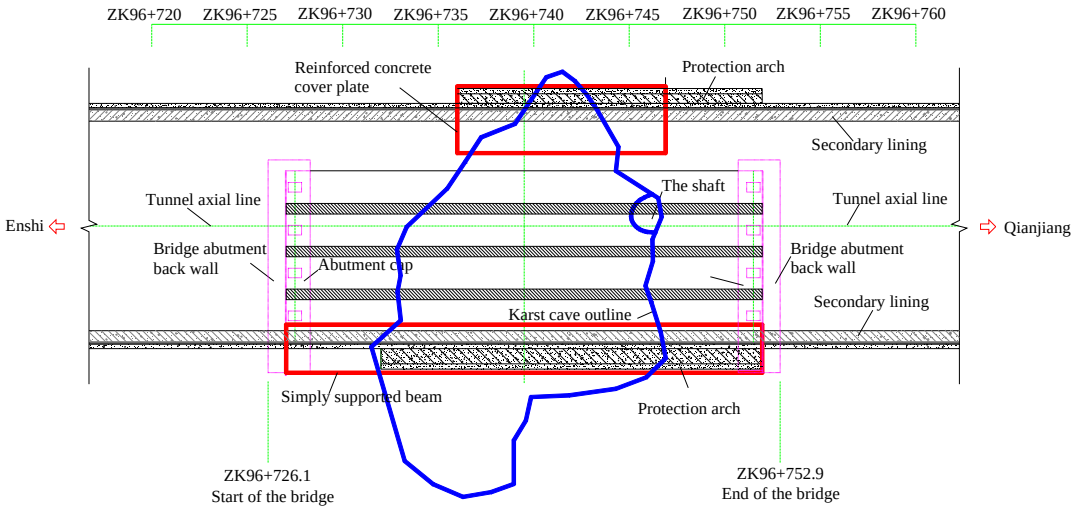

Figure 8. The layout plan of the treatment.

A rectangular reinforced concrete pre-stressed beam, which is the supporting beam of the protection arch, was arranged at the right arch foot. A reinforced concrete cover plate was arranged at the left arch foot.

The protection arch was composed of three layers. The outer layer of the protection arch consisted of I22b joint steel with a longitudinal spacing of 0.5 m, ϕ8 steel mesh with a spacing of 20 cm × 20 cm, and 28-cm thick C20 shotcrete. The 5-m long steel bars were installed at the outer portion of the protection arch each time, and part of the longitudinal reinforcing steel bars were reserved for lapping. The inner layer of the protection arch consisted of I18 joint steel with longitudinal spacing of 1.0 m, ϕ8 steel mesh with a spacing of 25 cm × 25 cm, and 24 cm thick C20 shotcrete. There were five reserved holes, each 2 m in a circular direction for vibrating the arch concrete. The middle layer was a 50-cm thick reinforced concrete arch. The concrete pouring construction proceeded synchronously from the left and right side through the reserved holes and the height difference between the two sides should be less than 1 m. The concrete should be well vibrated at different layers by using insertion-type vibrators. The insertion depth into the lower layer was not less than 10 cm each time.

During the support construction of the outer layer protection arch, an advanced joist steel frame was adopted as a safety protection measure within the scope of 120° at the arch. The joist steel used by the frame was I20 type and 4–5 m long. The frame and the outer layer steel was welded together. The lapped length was 1 m. The spacing in the ring direction was 40 cm. The frame was laid with ϕ8 steel mesh with a spacing of 20 cm × 20 cm and closed by C20 shotcrete, which could prevent the risk of dropping stones.

The construction of the buffer layer is synchronized with the construction of the outer layer protection arch by means of heaping up with old tires. ϕ22 steel bars, 5.5 m in radius with a spacing of 1.0 m in the ring direction were reserved when installed with the joist steel of the outer protection arch. The steel bars served as fixed piles of the backfill material. The old tires were stacked up and strung together along the contour of the outer layer of the protection arch. The stack thickness of the buff layer was 2.5 m.

(3) The Construction of the Pre-Stressed Reinforced Concrete T Bridge

The pavement of the tunnel used a bridge to cross the karst cave areas. The bridge had only a span of 25.0 m. The bridge was composed of four pre-stressed concrete simply-supported T beams. The bridge abutment was the light spread foundation type. The foundation and the surrounding rock were consolidated together by using anchors. D80 expansion joints were used in the bridge abutment.

(4) The Secondary Liner Construction

The second lining adopted 60-cm thick C25 reinforced concrete. There was a 35 cm reserved deformation space between the second lining and the protection arch. Considering the convenience of construction, the reserved space was filled with hard foam.

6. Conclusions and Discussion

Based on statistical analyses and analytic hierarchy process, the influence factors and their weights of the surrounding rock stability of the tunnel with a concealed karst cave in the west of the Hubei mountainous area expressway are studied. The results show that: surrounding rock grades, supporting measures, formation lithology, unfavorable geology, construction methods, blasting techniques, advanced geological forecasts, and groundwater levels are the main controlling factors. Topography and landform, attitude of stratum, monitoring measures, strata combination, and interlayer fissures are the minor factors. Finally, tunnel section shapes, in situ stress, and geological logging methods are the least important factors.

An assessment method of the influence of the concealed karst cave on rock stability surrounding the tunnel is proposed. The method can provide a theoretical basis to the stability analysis of the surrounding rock, scheme designs of treatment, and construction organization designs. It can also control the construction risks effectively and exactly in real-time in karst tunnels, which can achieve dynamic modification and management of the risks.

The established tunnel stability assessment model is applied in the assessment of a concealed karst cave's influence on the stability of the Huaguoshan karst tunnel on the Enshi-laifeng and Enshi-Qianjiang Expressways. The evaluation result agrees well with the site situation of construction that verifies the feasibility and practicality of using the analytic hierarchy process to assess the stability of the surrounding rock of the tunnel. It can also correctly guide the construction.

A four stage construction method was used to treat the karst cave at ZK96 + 476 of the Huaguoshan Tunnel. The method includes backfill of the karst cave shaft, the construction of the protection arch, the bridge crossing the shaft construction, and the secondary lining construction. The karst cave was successfully treated, at last. The treatment experience can provide an important reference to similar engineering.

Nevertheless, this research has several limitations. Firstly, the results are based on 207 concealed karst caves in 21 tunnels of Enshi-Laifeng and Enshi-Qianjiang Expressways in Western Hubei Province. Different engineering and karst regions have their own particularity. Although this method is successful applied to the provided engineering, more applications in different karst areas should be taken to verify the correctness of the result. Secondly, the assessment model takes sufficient influence factors into consideration, therefore, abundant and accurate engineering data are crucial during the evaluation process. Finally, the weights of the influence factors of the assessment model are different in different construction stages. This research mainly focuses on the stage before the karst cave is treated. Evaluating the stability of the rock surrounding the tunnel during the karst cave treatment stage is one of the future research directions.

Author Contributions: Zhenhao Xu, Xin Huang and Shucai Li conceived, designed and performed the research; Xin Huang and Ming Guo wrote the paper and analyzed the data; and Yucheng Chen performed the field work and provided advice with respect to the engineering application.

Funding: This work was supported by the National Natural Science Foundation of China (Grant No.: 51509147), the Fundamental Research Funds of Shandong University (Grant No.s: 2017JC002, 2017JC001).

Conflicts of Interest: The authors declare no conflict of interest.

References

1. Li, S.C.; Xu, Z.H.; Huang, X.; Lin, P.; Zhao, X.C.; Zhang, Q.S.; Yang, L.; Zhang, X.; Sun, H.F.; Pan, D.D. Classification, geological identification, hazard mode and typical case studies of hazard-causing structures for water and mud inrush in tunnels. *Chin. J. Rock Mech. Eng.* **2018**, *37*, 1041–1069. [CrossRef]

2. Lu, Y.R.; Liu, Q.; Zhang, F.E. Environmental characteristics of karst in China and their effect on engineering. *Carbonates Evaporites* **2013**, *28*, 251–258. [CrossRef]
3. Wang, Y.C.; Jing, H.W.; Yu, L.Y.; Su, H.; Luo, N. Set pair analysis for risk assessment of water inrush in karst tunnels. *Bull. Eng. Geol. Environ.* **2017**, *76*, 1199–1207. [CrossRef]
4. Parise, M.; Waele, J.D.; Gutierrez, F. Engineering and environmental problems in karst—An introduction. *Eng. Geol.* **2008**, *99*, 91–94. [CrossRef]
5. Gutiérrez, F.; Parise, M.; Waele, J.D.; Jourde, H. A review on natural and human-induced geohazards and impacts in karst. *Earth Sci. Rev.* **2014**, *138*, 61–88. [CrossRef]
6. Marinos, P.G. Tunnelling and mining in karstic terrain: An engineering challenge, geotechnical and environmental applications of karst geology and hydrology. In Proceedings of the 8th Multidisciplinary Conference on Sinkholes and the Engineering and Environmental Impacts of Karsts, Louisville, Kentucky, 1–4 April 2001.
7. Alija, S.; Torrijo, F.J.; Ferreira, M.Q. Geological engineering problems associated with tunnel construction in karst rock masses: The case of Gavarres tunnel (Spain). *Eng. Geol.* **2013**, *157*, 103–111. [CrossRef]
8. Eskesen, S.D.; Tengborg, P.; Kampmann, J.; Veicherts, T.H. Guidelines for tunnelling risk management: International tunnelling association, working group No. 2. *Tunn. Undergr. Space Technol.* **2004**, *19*, 217–237. [CrossRef]
9. Song, K.I.; Cho, G.C.; Chang, S.B. Identification, remediation, and analysis of karst sinkholes in the longest railroad tunnel in South Korea. *Eng. Geol.* **2012**, *135–136*, 92–95. [CrossRef]
10. Knez, M.; Slabe, T. Karstology and the opening of caves during motorway construction in the karst region of Slovenia. *Int. J. Speleol.* **2002**, *31*, 159–168. [CrossRef]
11. Day, M.J. Karstic problems in the construction of Milwaukee's deep tunnels. *Environ. Geol.* **2004**, *45*, 859–863. [CrossRef]
12. Zarei, H.R.; Uromeily, A.; Sharifzadeh, M. Identifying geological hazards related to tunneling in carbonate karstic rocks—Zagros, Iran. *Arba. J. Geosci.* **2012**, *5*, 457–464. [CrossRef]
13. Koutepov, V.M.; Mironov, O.K.; Tomachev, V.V. Assessment of suffosion-related hazards in karst areas using GIS technology. *Environ. Geol.* **2008**, *54*, 957–962. [CrossRef]
14. Zhao, Y.; Li, P.F.; Tian, S.M. Prevention and treatment technologies of railway tunnel water inrush and mud gushing in China. *J. Rock Mech. Geotech. Eng.* **2013**, *5*, 468–477. [CrossRef]
15. Cui, Q.L.; Wu, H.N.; Shen, S.L.; Xu, Y.S.; Ye, G.L. Chinese karst geology and measures to prevent geohazards during shield tunnelling in karst region with caves. *Nat. Hazards* **2015**, *77*, 129–152. [CrossRef]
16. Casagrande, G.; Cucchi, F.; Zini, L. Hazard connected to railway tunnel construction in karstic area: Applied geomorphological and hydrogeological surveys. *Nat. Hazards Earth Syst. Sci.* **2005**, *5*, 243–250. [CrossRef]
17. Zhao, Y.L.; Peng, Q.Y.; Wan, W.; Wang, W.J.; Chen, B. Fluid-solid coupling analysis of rock pillar stability for concealed karst cave ahead of a roadway based on catastrophic theory. *Int. J. Rock Mech. Min.* **2014**, *24*, 737–745.
18. Li, S.C.; Lin, P.; Xu, Z.H.; Li, L.P.; He, S.J.; Zhao, S.L.; Huang, X. Innovative method for the integral sliding stability analysis of filling media in karst caves and its applications in engineering. *Int. J. Geomech.* **2017**. [CrossRef]
19. Xu, Z.H.; Wu, J.; Li, S.C.; Zhang, B.; Huang, X. Semianalytical solution to determine minimum safety thickness of rock resisting water inrush from filling-type karst caves. *Int. J. Geomech.* **2018**. [CrossRef]
20. Li, X.P.; Li, Y.N. Research on risk assessment system for water inrush in the karst tunnel construction based on GIS: Case study on the diversion tunnel groups of the Jinping II Hydropower Station. *Tunn. Undergr. Space Technol.* **2014**, *40*, 182–191. [CrossRef]
21. Meng, Z.P.; Li, G.Q.; Xie, X.T. A geological assessment method of floor water inrush risk and its application. *Eng. Geol.* **2012**, *143*, 51–60. [CrossRef]
22. Wang, J.; Li, S.C.; Li, L.P.; Lin, P.; Xu, Z.H.; Gao, C.L. Attribute recognition model for risk assessment of water inrush. *Bull. Eng. Geol. Environ.* **2017**. [CrossRef]
23. Zhou, Z.Q.; Li, S.C.; Li, L.P.; Shi, S.S.; Xu, Z.H. An optimal classification method for risk assessment of water inrush in karst tunnels based on the grey system. *Geomech. Eng.* **2015**, *8*, 631–647. [CrossRef]
24. Li, S.C.; Zhou, Z.Q.; Li, L.P.; Xu, Z.H.; Zhang, Q.Q.; Shi, S.S. Risk assessment of water inrush in karst tunnels based on attribute synthetic evaluation system. *Tunn. Undergr. Space Technol.* **2013**, *38*, 50–58. [CrossRef]

25. Li, S.C.; Wu, J.; Xu, Z.H.; Zhou, L.; Zhang, B. A possible prediction method to determine the top concealed karst cave based on displacement monitoring during tunnel construction. *Bull. Eng. Geol. Environ.* **2017**. [CrossRef]
26. Kim, D.S.; Lee, H.C.; Suh, Y.H.; Ryu, C.H. Railway tunnel design against karstic collapse in Korea. In Proceedings of the Conference on ISRM 2003–Technology Roadmap for Rock Mechanics, South African Institute of Mining and Metallurgy, Sandton, South Africa, 8–12 September 2003.
27. Yang, X.L.; Xiao, H.B. Safety thickness analysis of tunnel floor in karst region based on catastrophe theory. *J. Cent. South Univ.* **2016**, *23*, 2364–2372. [CrossRef]
28. Fraldi, M.; Guarracino, F. Limit analysis of collapse mechanisms in cavities and tunnels according to the Hoek–Brown failure criterion. *Int. J. Rock Mech. Min.* **2009**, *46*, 665–673. [CrossRef]
29. Parise, M.; Lollino, P. A preliminary analysis of failure mechanisms in karst and man-made underground caves in southern Italy. *Geomorphology* **2011**, *134*, 132–143. [CrossRef]
30. Pesendorfer, M.; Loew, S. Subsurface exploration and transient pressure testing from a deep tunnel in fractured and karstified limestones. *Int. J. Rock Mech. Min.* **2010**, *47*, 121–137. [CrossRef]
31. Criss, E.M.; Criss, R.E.; Osburn, G.R. Effect of stress on cave passage shape in karst terranes. *Rock Mech. Rock Eng.* **2008**, *41*, 499–505. [CrossRef]
32. Guo, M. Study on Concealed Karst Cave's Influence on Karst Tunnel Stability and Treatment Technology on Tunnels of E-xi Mountainous. Master's Thesis, Shandong University, Jinan, China, 2014.
33. Jiang, C.; Zhao, M.H.; Cao, W.G. Stability analysis of subgrade cave roofs in karst region. *J. Cent. South Univ. Technol.* **2008**, *15*, 38–44. [CrossRef]
34. Huang, F.; Zhao, L.H.; Ling, T.H.; Yang, X.L. Rock mass collapse mechanism of concealed karst cave beneath deep tunnel. *Int. J. Rock Mech. Min.* **2017**, *91*, 133–138. [CrossRef]
35. Knez, M.; Slabe, T.; Šebela, S.; Gabrovšek, F. The largest karst cave discovered in a tunnel during motorway construction in Slovenia's Classical Karst (Kras). *Environ. Geol.* **2008**, *54*, 711–718. [CrossRef]
36. Wang, Y.; Sun, C.H. Forecasting model of safe thickness for roof of karst cave under highway tunnel. *Highway* **2006**, *5*, 228–232.
37. Bian, X.L.; Chen, F.Q.; Su, F.; Sun, S.W. Mechanical characteristics analysis of surrounding rock in deep buried tunnel in karst regions. *China Railw. Sci.* **2013**, *34*, 43–49.
38. Saaty, T.L. Applications of analytical hierarchies. *Math. Comput. Simul.* **1979**, *21*, 1–20. [CrossRef]
39. Saaty, T.L. How to make a decision: The analytic hierarchy process. *Eur. J. Oper. Res.* **1990**, *48*, 9–26. [CrossRef]
40. Xu, Z.H.; Li, S.C.; Li, L.P.; Hou, J.G.; Sui, B.; Shi, S.S. Risk assessment of water or mud inrush of karst tunnels based on analytic hierarchy process. *Rock Soil Mech.* **2011**, *32*, 1757–1766.